ELSEVIER

Contents lists available at ScienceDirect

# Journal of Colloid and Interface Science

journal homepage: www.elsevier.com/locate/jcis



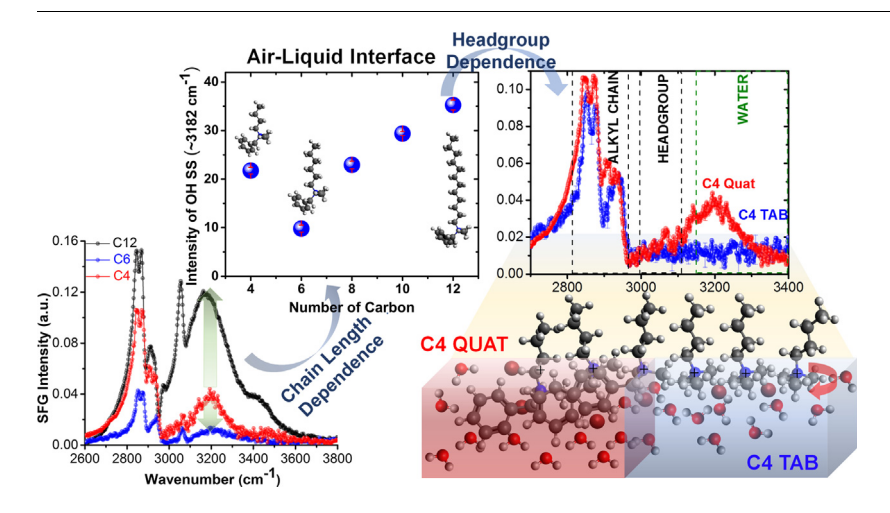
# Role of the cationic headgroup to conformational changes undergone by shorter alkyl chain surfactant and water molecules at the air-liquid interface



Md. Rubel Khan, Uvinduni I. Premadasa, Katherine Leslee A. Cimatu\*

Department of Chemistry and Biochemistry, Ohio University, 100 University Terrace, 136 Clippinger Laboratories, Athens, OH 45701-2979, United States

#### G R A P H I C A L A B S T R A C T



## ARTICLE INFO

Article history: Received 16 December 2019 Revised 13 February 2020 Accepted 14 February 2020 Available online 15 February 2020

Keywords:
Cationic surfactant
Corrosion
SFG spectroscopy
Air-liquid interface
Chain length
lonic strength
Adsorption
Surface tension

## ABSTRACT

*Hypothesis*: Surfactants are commonly used as corrosion inhibitors for oil-and-gas pipelines. The alkyl chain of surfactants and their overall conformation contributes to the adsorption, flotation, and foam separation in the inhibition process. We hypothesize that the conformation of shorter alkyl chains and chemical nature of surfactants has an effect on the ordering of water molecules at the air-water interface which is not yet well understood.

*Experiments:* Alkyl (C4, C6, C8, C10, and C12) dimethylbenzylammonium bromides (Quats) were synthesized. Aqueous solutions at 0% and with different salt concentrations were studied at the air-liquid interface using sum frequency generation spectroscopy. Surface tension and pH measurement were also conducted for comparison.

Findings: Surfactant solutions at 0%, 1%, and 10% salt showed a zigzag trend for the number of gauche defects. At 0% salt, an increasing trend of OH band intensity at 3182 cm<sup>-1</sup> was observed from C6 to C12 SFG spectra. Yet, C4 showed a more prominent SFG signal from strongly hydrogen-bonded water molecules compared to C6. The headgroup's chemical nature was found to play a role in the ordering of water molecules for a C4 alkyl chain length. The OH band intensity decreases with increasing ionic strength.

© 2020 Elsevier Inc. All rights reserved.

E-mail address: cimatu@ohio.edu (K.L.A. Cimatu).

<sup>\*</sup> Corresponding author.

#### 1. Introduction

Surfactants are useful in applications such as corrosion inhibition, soaps, paints, adhesives, inks, insecticides, antibacterial, antifungal, and many other applications [1–3]. Depending on the application, surfactant molecules are being constantly modified to serve a specific purpose under specific conditions. The combined use of surface tension and SFG shall help us understand how alkyl chain length and ionic strength affect the self-assembly, surface coverage, and CMC of surfactants. These fundamental studies of surfactants at the air-water interface will provide novel insights to design new surfactants for a specific field of application.

Surfactants are widely employed as corrosion inhibitors to protect metal surfaces of pipelines in the oil-and-gas industry due to their low toxicity, high solubility, high hydrocarbon content, and ability to adsorb onto metals to retard corrosion [4–10]. These surfactants can react with the impurities of the metal surface or restrict the rate of the anodic or cathodic processes by simply blocking the active sites or pits present on metal surfaces [9]. The most commonly used inhibitors are from groups of amines, amides, quaternary ammonium salts, imidazolines, aromatic aldehydes, acetylenic alcohols, condensation products of carbonyls, and alkyltrimethylammonium-based surfactants [6.11–14]. These compounds are amphiphilic by nature, which contain a hydrophilic headgroup and a hydrophobic chain group. As the headgroup adsorbs on the metal surface forming a self-assembled monolayer, the alkyl chain group arranges itself towards the bulk solution and provides a barrier for corrosive substances like water and dissolved gases (CO<sub>2</sub> and SO<sub>2</sub>) using electrochemical impedance spectroscopy [4,11]. Thus, these surfactants become good candidates for corrosion inhibition [15].

Both head and alkyl chain groups play an important role in conformational changes of surfactants at air-liquid and solid-liquid interfaces [16,17]. In water-soluble surfactants, the chain groups project to the air and the headgroup points to the interfacial water at the air-water interface. The presence of charged surfactants at the air-water interface shows an overall enhancement of hydroxy (OH) peaks of interfacial water molecules [18]. Charged surfactants can create a large electrostatic field in the double-layer region. In this scenario, interfacial water molecules orient themselves with the hydrogen of OH bands pointing down for cationic surfactants, whereas the hydrogen of OH bands for anionic surfactants is pointing up [19]. The previous works on conformational changes of surfactants and water molecules by varying the headgroup, alkyl chain group, concentration, and ionic strength using sum frequency generation (SFG) spectroscopy have not yet reported the combined influences of the above-mentioned factors [16,20-25]. However, the chain length dependence of highly soluble surfactants with fewer carbons (C4-C12) at various salt concentrations in water has not yet been extensively studied at the air-liquid interface. Most of these surfactants do not reach CMC even at a high concentration which is the key factor for maximum surface coverage. The interfacial behavior of salt-water-surfactant at different chain lengths studied by surface-specific sum frequency generation spectroscopy (SFG) will be of great interest. As surfactants in water create an electrostatic field which greatly orients water molecules at the interfacial and double-layer regions, the presence of salt disturbs the hydrogen-bonding network of water [26]. The combined influences of the chain length and ionic strength in water should provide new insights in adsorption, selfassembly, and interfacial process like corrosion.

Independent studies on chain length and ionic strength in both air-solid and air-liquid interfaces state that as the number of carbon atom increases, a decrease in the number of gauche defects within the alkyl chains is expected [23,24]. Another study, per-

formed by Richmond and co-workers, reported a decreasing number in gauche conformations with decreasing chain length at the liquid-liquid interface [25]. In some other cases, such as studies with neat ionic liquids, it has been observed that the relative number of gauche defects increases with increasing chain length [20,27] On the other hand, the ionic strength dependence shows that the intensity of the OH stretch band positioned at ~3200 cm<sup>-1</sup> of the interfacial water at a charged surface decreases with increasing salt concentration due to the screening effect [18,28-31]. Thus, very few studies were performed that mainly focused on varying the chain length from C4- C12 in the absence and presence of inorganic salt at the air-water interface. In addition, studies on increasing chain length are somehow inconclusive when the number of gauche defects is concerned at different interfaces. Thus, it becomes noteworthy to learn how the conformation of shorter-chained surfactants and water molecules are arranged at the air-liquid interface in relation to their ability to form a wellordered monolayer, for the same reason that shorter chain alkyl surfactants are more soluble in water and becomes an ideal inhibitor because of its solubility properties. The insight it provides is important especially for applications such as corrosion inhibition.

In this study, we investigated conformational changes and monitored spectral profiles of quaternary-based ammonium surfactants with varying chain lengths from C4-C12 in aqueous solution, and varying salt (NaCl) concentrations at the air-water interface in CH and OH regions by SFG spectroscopy. SFG spectra were acquired from 2800 cm<sup>-1</sup> to 3700 cm<sup>-1</sup> with ssp and ppp polarization combinations. Each SFG spectrum was fitted to extract amplitude and intensity values in order to estimate gauche defects between the ratio of the methyl symmetric stretch (CH<sub>3</sub> SS) and the methylene symmetric stretch (CH<sub>2</sub> SS) and to determine the average tilt angle value of CH<sub>3</sub> group for the C4 Quat molecule. The fitted values were also useful in plotting the OH stretch as a function of chain length as well as salt concentration. Surface tension measurements were also performed for most of the aqueous solutions of the surfactant to estimate the surface coverage and find its correlation with SFG results.

#### 1.1. SFG theory

Sum frequency generation (SFG) spectroscopy is a surface-specific vibrational technique that obtains the vibrational spectra of the interfacial molecules [32]. The spectral analysis provides information about identification, conformation, and dynamics of interfacial molecules [33–36]. SFG spectroscopy provides molecular surface specificity and sub-monolayer sensitivity. It involves a nonlinear optical process in which its intrinsic symmetry requirement dictates that SFG can only arise from an interface, noncentrosymmetric bulk crystals, or bulk chiral molecules [36]. The centrosymmetry of the bulk can be explained by the isotropic distribution of molecules, and thus this results in no SF signal arising from the bulk. However, this symmetry breaks at the interface, thus creating an asymmetric environment for these interfacial molecules and becomes SF active.

The SFG signal is generated at the sample surface from the temporal and spatial overlap of the two pulsed laser beams. One laser beam is the visible beam with the frequency;  $\omega_{\text{VIS}}$  and the other beam is the mid-infrared beam with tunable frequency;  $\omega_{\text{IR}}$  and the sum of the two frequencies results in the generated output beam of the SFG process ( $\omega_{\text{SF}}$ ).

$$\omega_{SF} = \omega_{VIS} + \omega_{IR} \tag{1}$$

SFG intensity is directly proportional to the square of the effective second-order nonlinear susceptibility, with the incident fixed 795 nm and tunable mid-IR beams.

$$I_{(\omega_{SF})} \propto \left[ \sum_{i} \chi_{eff}^{(2)} \sum_{i,k} E_{j} E_{k} \right]^{2}$$
 (2)

Herein,  $I_{(\omega_{SF})}$  is the SFG intensity and  $\chi^{(2)}$  is the effective second-order nonlinear susceptibility.  $\chi^{(2)}_{\rm eff}$  is a third rank tensor which can be further defined by using Fresnel factors and the macroscopic nonlinear susceptibilities,  $\chi^{(2)}_{ijk}$ , at the interface, as shown in Eq. (3).

$$\chi_{\text{eff,ijk}}^{(2)} = \chi_{\text{iik}}^{(2)} [L_i e_i] [L_j e_j] [L_k e_k]$$
(3)

Where i, j, and k coordinates represent x, y, z-axes, respectively. L represents the Fresnel factor while e represents the unit optical field vector. The macroscopic susceptibility has 27 components, but due to symmetry constraints obtained at the surface, some of the components become almost negligible. Therefore, there are only 7 components left, which correspond to four possible polarization combinations; ssp, ppp, pss, and sps. SFG spectra were collected at ssp and ppp polarization combinations only. The beam polarizations s and p refer to incident beam perpendicular and parallel to the plane of incidence, respectively [28]. The three beams are listed in the order of decreasing energy; ssp refers to the SFG beam is (s) polarized, visible beam is (s) polarized, and the mid-IR beam is (p) polarized.

 $\chi^{(2)}_{\rm eff}$  is composed of the resonant susceptibility,  $\chi^{(2)}_{\rm R}$ , and the non-resonant susceptibility,  $\chi^{(2)}_{\rm NR}$ .

$$\chi_{\rm eff}^{(2)} = \chi_{\rm R}^{(2)} + \chi_{\rm NR}^{(2)}$$
 (4)

The nonresonant term,  $\chi_{NR}^{(2)}$ , depends on the surface plasmon resonance of the substrate and is also found to be invariant with IR frequency [33].  $\chi_{NR}^{(2)}$  is almost negligible for liquid and dielectric surfaces.

$$\chi_{R}^{(2)} = \sum_{q} \frac{N \langle \beta^{(2)} \rangle}{(\omega_{IR} - \omega_{q} + i\Gamma_{q})}$$
 (5)

The resonant term,  $\chi_R^{(2)}$ , as shown in Eq. (5), is due to vibrational transitions of the interfacial molecules. N is the number density of vibrational modes,  $\beta^{(2)}$  is the orientational averaged hyperpolarizability, and  $\Gamma_q$  is the damping constant of  $q^{th}$  vibrational mode, respectively. $\omega_{IR}$ ,  $\omega_q$  are the IR frequency and the frequency of the  $q^{th}$  vibrational mode, respectively [32].

#### 2. Experimental details

# 2.1. Synthesis and purification of alkylbenzyldimethylammonium bromide (Quats)

Alkylbenzyldimethylammonium bromides containing five different alkyl chain lengths butyl (C4), hexyl (C6), octyl (C8), decyl (C10), and dodecyl (C12) were synthesized using established methods [28,37]. 0.100 mol of N,N-dimethylbenzylamine (Fisher Scientific, New Hampshire, US) and 100 ml of acetonitrile (Fisher Scientific, New Hampshire, US) were added into the three-necked round-bottom flask. After that, the solution in the round-bottom flask was heated to a reflux temperature of 82 °C. At ~82 °C, 0.100 mol (equimolar) of bromoalkane (Fisher Scientific, New Hampshire, US) was added dropwise to the solution, Refluxing was continued for 24 h. The solvent was recovered from the reaction mixture by rotary evaporation. Finally, the trace amount of solvent and colored impurities were removed by recrystallization process with deionized water. A solid crystalline Quat was obtained for C4, C6 and C8 and viscous liquid for C10 and C12. The structure and the purity of synthesized Quats were confirmed by <sup>1</sup>H NMR spectra with their corresponding purity values available in Table S1 of the Supporting Information (SI) [28].

#### 2.2. Instrumentation

The SFG set-up utilized Solstice broadband femtosecond Titanium-Sapphire laser from Spectra-Physics (Santa Clara, CA), which generated the fundamental beam at 795 nm. The detailed experimental set-up was described in the earlier publications of the group [32,38]. The 795 nm visible output beam was sent to a 50:50 beamsplitter. The 50% reflected beam passed through a Fabry-Pérot etalon to generate the narrow bandwidth visible beam. The 50% transmitted beam was sent to an optical parametric amplification system (TOPAS-C) and difference frequency generation (DFG) crystal to generate the broadband mid-infrared beam. Both visible and IR beams were temporally and spatially overlapped at the sample surface with incident angles of 50° and 60°, respectively, which generated the SFG beam at 52° from the surface normal. Then the SFG beam was collected through a spectrograph and a charge-coupled device camera.

#### 2.3. Sample preparation

Eicosanoic acid (EA) with >99% was purchased from Sigma Aldrich (St. Louis MO) and used as received. 2 mg of EA was dissolved in 1 ml of chloroform. 25 µl of this solution was used to form a monolayer in a petri dish containing 60 ml of deionized water. Self-assembled EA monolayer on the water was used as a reference sample for the SFG signal optimization at the air-liquid interface. The SFG spectrum was collected using the ssp polarization combination [32,38]. 8.0 mM aqueous solutions (60 ml) in deionized H<sub>2</sub>O (18 MOhm cm) were prepared for the five Quats compounds (C4, C6, C8, C10, and C12) with 0%, 1% and 10% (w/w) of sodium chloride (NaCl). Additional solutions with 0.5% and 5% sodium chloride were prepared for the C8 Quat compound. Freshly prepared samples were sonicated for ~20 min. The EA solution in a glass Petri dish was replaced by an equal volume of Quat aqueous solution in a similar glass Petri dish and equilibrated for 30 min prior to collecting SFG spectral data.

#### 2.4. Data acquisition

The gold and polystyrene films were used to optimize the overlap of the two beams and to calibrate the x-axis for the IR frequency, respectively. Gold spectra were collected at ten IR centers for every 100 cm<sup>-1</sup> from 2800 cm<sup>-1</sup> to 3700 cm<sup>-1</sup> with one-second acquisition time. All spectra were backgroundcorrected and stitched together. SFG spectra of the five quaternary ammonium bromide samples were also acquired at ten IR centers from  $2800 \text{ cm}^{-1}$  to  $3700 \text{ cm}^{-1}$  at every  $100 \text{ cm}^{-1}$  to probe the entire CH and OH regions using ssp and ppp polarization combinations. Three trials and background were collected for each run. Then, each trial was collected for 9 min (3-sec acquisition time for 180 accumulations). Each summed spectrum was corrected for the polarization efficiency of the optics and the data used for fitting and orientational analysis from 2800 cm<sup>-1</sup> to 3700 cm<sup>-1</sup> using Eqs. (6) and (7) [38]. A plot is available in the Supporting Information, as Fig. S1, which contains a series of individual spectrum collected from every IR center including the summed

The energies of the visible beam and IR beam were measured to be  $\sim$ 26  $\mu$ J and  $\sim$ 8  $\mu$ J, respectively, at the sample stage.

### 2.5. Fitting equation

The following Lorentzian line shape equation is considered to analyze each polarization combination and also accounts for the line broadening.

$$I_{SFG} \propto \left|\chi^{(2)}\right|^2 \propto \left|\sum_{q} \frac{N\langle\beta^{(2)}\rangle}{(\omega_{IR} - \omega_q + i\Gamma_q)} + \left|\chi_{NR}^{(2)}\right|e^{i\rho}\right|^2$$
 (6)

Where  $\rho$  is the phase of the nonresonant response. The nonresonant contribution from the bulk and the Gaussian equation are both included in the fitting equation to account for the midinfrared beam's broadband pulse width Eq. (7). This simplified version of the fitting equation that accounts for the CH and OH vibrational modes is presented below.

$$\begin{split} I_{SFG}(\omega + \omega_{vis}) &\propto exp \left[ -\frac{(\omega - \omega_{IR}^L)^2}{2(\delta \omega_L)^2} \right] \\ &\times \left| \sum_q \frac{A_q}{\omega_{IR} - \omega_q + i\Gamma_q} + A_{NR} e^{i\rho} \right|^2 \end{split} \tag{7}$$

where 
$$\left|\sum_{q} \frac{A_{q}}{\omega_{lR} - \omega_{q} + i\Gamma_{q}}\right|^{2} = \left|\sum_{CH} \frac{A_{CH}}{\omega_{lR} - \omega_{CH} + i\Gamma_{q}} + \sum_{OH} \frac{A_{OH}}{\omega_{lR} - \omega_{OH} + i\Gamma_{q}}\right|^{2}$$
  
The Gaussian curve equation is defined with the spectral width

The Gaussian curve equation is defined with the spectral width  $\delta\omega_L$  centered at  $\omega_R^L$ . The spectral width  $\delta\omega_L$  centered at  $\omega_R^L$  is included in the Gaussian function. The amplitude factors,  $A_q$  and  $A_{NR}$ , are proportional to the molecular hyperpolarizabilities as shown above in Eq. (7). The amplitudes,  $A_{CH}$  and  $A_{OH}$ , and frequency positions,  $\omega_{CH}$  and  $\omega_{OH}$ , result from CH and OH vibrational modes.

#### 3. Results and discussion

As discussed above, the quaternary ammonium bromides (Quats) surfactants of interest for this study are Quats with 4, 6, 8, 10, and 12 carbons for the hydrophobic portion of the amphiphilic compound. Since these Quats are useful in preventing internal corrosion of oil-and-gas transportation pipelines, an insight towards its adsorption, self-assembly, and behavior at an interface is beneficial towards understanding the role of these shorter chain length surfactants in an aqueous phase.

#### 3.1. Peak assignments

8.0 mM solutions of five Quats in H<sub>2</sub>O (~60 ml) were characterized at the air-liquid (AL) interface by SFG spectroscopy. Fig. 2 shows the SFG spectra taken at the ssp and ppp polarization combinations. The vibrational modes arise from the terminal methyl and methylene groups of the chain (C4-C12), the two ammonium methyl groups, and benzyl unit of the headgroup (Fig. 1), and OH stretching modes of hydrogen-bonded water molecules. The Quat and water molecules were probed in CH and OH regions. Detailed peak assignments were described in an earlier publication [28]. The peaks of the ssp spectrum (Fig. 2a) are assigned from left to right, first two peaks can be assigned to the methylene symmetric stretch (CH<sub>2</sub> SS) at ~2851 cm<sup>-1</sup> [39,40] and the terminal methyl symmetric stretch (CH<sub>3</sub> SS) at ~2876 cm<sup>-1</sup> [39-42]. The next two peaks can then be assigned to the methylene asymmetric stretch (CH<sub>2</sub> AS) at ~2915 cm<sup>-1</sup> and the methyl Fermi resonance (CH<sub>3</sub> FR) at ~2936 cm<sup>-1</sup>. Fermi resonance mode is due to the Fermi

Fig. 1. Quaternary ammonium bromides (Quats), where n = 4, 6, 8, 10, and 12.

interaction of the CH<sub>3</sub> SS and the overtone of the methyl bending mode [35,39,40].

The peaks observed at ~2978 cm<sup>-1</sup> and ~3058 cm<sup>-1</sup> were assigned to ammonium methyl symmetric stretch (N-CH<sub>3</sub> SS) and ammonium methyl asymmetric stretch (N-CH<sub>3</sub> AS) or the combination of aromatic CH stretch and N-CH<sub>3</sub> AS, respectively [43,44]. The peaks at ~3182 cm<sup>-1</sup> and ~3384 cm<sup>-1</sup> are assigned as OH stretching modes for tetrahedrally and asymmetrically hydrogen-bonded water molecular arrangements, respectively [45–48].

In the ppp polarization combination in Fig. 2b, the peaks positioned at ~2857 cm $^{-1}$ , ~2889 cm $^{-1}$ , ~2915 cm $^{-1}$ , and ~2961 cm $^{-1}$  were assigned to methylene Fermi resonance (CH $_2$  FR) [39], terminal methyl symmetric stretch (CH $_3$  SS), methylene asymmetric stretch (CH $_2$  AS), and methyl asymmetric stretch (CH $_3$  AS), respectively [40,49]. The CH $_3$  SS in the ppp spectrum is shifted by ~13 cm $^{-1}$  compared to ssp spectrum due to Fermi interactions with the overtone of the CH $_3$  bending vibrations, causing unequal SFG intensity redistribution [50–52]. A summary of the peak assignments is available in Table 1.

The antisymmetric v<sub>20b</sub> mode of the phenyl group was observed at  $\sim 3022 \text{ cm}^{-1}$  [53]. The peak positioned at  $\sim 3066 \text{ cm}^{-1}$  can be either assigned to ammonium methyl asymmetric stretch (N-CH<sub>3</sub> AS)[54] or the symmetric  $v_2$  resonance of the phenyl group [53] or the combination of the two modes. Both the OH stretching modes of water were also observed in the ppp polarization combination [45,46,48]. In neat water, signal arises from contributions of different OH bands of interfacial water molecules including the free OH [31,48]. The addition of surfactants in water enhances the intensity of hydrogen-bonded OH bands due to the effect of surface electric field and provides adequate hydrogen bond acceptors for the interfacial water molecules which relatively reduces the number density of the free OH band [31,47,48,55]. Another reason behind the absence of free OH groups at the air-water interface might be due to more surfactant molecules are adsorbed compared to the number of interfacial water molecules [28]. At higher surfactant concentration, the surface coverage presents an almost full monolaver coverage at the air-water interface which results in reduced or almost no free OH groups [56]. Fig. S2 shows the combined SFG spectra 3600 cm<sup>-1</sup> and 3700 cm<sup>-1</sup>. As presented, only C8 Quat shows a free OH signal in the SFG spectrum. Again, the addition and the number density of surfactants have affected the low contribution of the free OH signal at the air-liquid interface. It is also important to note that after summing all SFG spectra from the 10 IR centers, the counts of the free OH in the C8 Quat is only about ~2.5% of the overall SFG signal and not prominent in the SFG spectrum from  $2800 - 3700 \text{ cm}^{-1}$ .

3.2. Is the conformation of the alkyl chain dependent on the length of Quat surfactants from C4-C12?

Five 8 mM aqueous solutions of Quat compounds with an alkyl chain length varying from C4, C6, C8, and C10–C12 were prepared for the spectral data acquisition. To test the effects of varying the chain length, we are first analyzing the SFG spectra of the 8 mM Quats in water for any change in the alkyl chain conformation. For well-ordered self-assembled monolayers, the alkyl chain has an all-trans conformation and their CH<sub>2</sub> groups lie in a centrosymmetric environment and thus becoming SF inactive [33]. The SF spectral profile of a well-ordered monolayer mainly contains the terminal CH<sub>3</sub> group vibrational modes whereas, for a not so well-ordered monolayer, the SF spectra comprise of vibrational contributions from CH<sub>3</sub> and CH<sub>2</sub> groups. This conformational disorder in the alkyl chain can be referred to as a gauche defect [33]. Previous studies reported that the extent of gauche defects in the structure of a surfactant monolayer increases with the chain length and

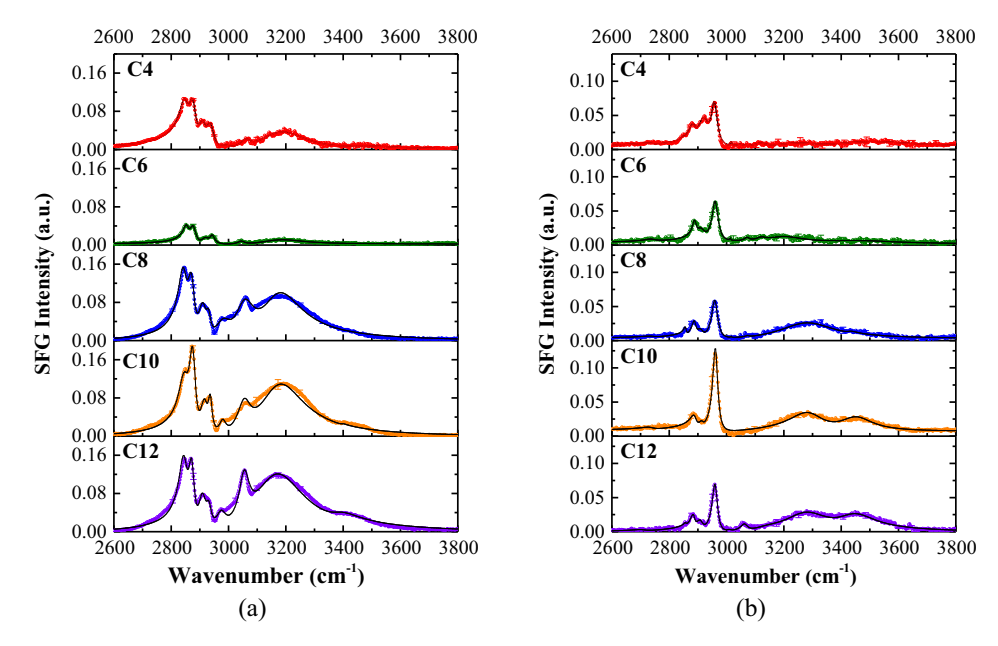


Fig. 2. Fitted SFG spectra of 8 mM C4, C6, C8, C10, and C12 Quat compounds in water (without NaCl) at (a) ssp and (b) ppp polarization combinations.

**Table 1**Peak assignments from the fitted SFG spectra of Quats at ssp and ppp polarization combinations.

Peak assignments	ssp Wavenumber (cm <sup>-1</sup> )	ppp Wavenumber (cm <sup>-1</sup> )
CH <sub>2</sub> SS	~2851	=
CH <sub>2</sub> FR	_	~2857
CH₃ SS	~2876	~2889
CH <sub>2</sub> AS	~2915	~2915
CH <sub>3</sub> AS	_	~2961
CH₃ FR	~2936	_
N-CH <sub>3</sub> SS	~2978	_
Aromatic CH stretch (v <sub>20b</sub> mode)	_	~3022
N-CH <sub>3</sub> AS/Aromatic CH stretch (v <sub>2</sub> mode)	~3058	~3066
OH SS	~3182	~3268
OH SS	~3384	~3451

then decreases for longer chains [57,58]. In these studies, the enhancement in the CH2 SS intensity was attributed to an increase in the conformational disorder. Another study reported that the ratio between CH3 SS to CH2 SS is inversely proportional to the degree of packing, which they found to be dependent on the chemical nature of the head group [16]. Therefore, to obtain a quantitative insight into the conformation of the Quat compounds at the air-liquid interface, the intensity ratio between CH<sub>2</sub> SS and CH<sub>3</sub> SS was calculated to measure the extent of relative disorder or gauche defects in the alkyl chain conformation [25]. The peak intensities of CH2 SS and CH3 SS modes were obtained from fitted ssp spectra in Fig. 2. A plot of CH<sub>2</sub> SS/CH<sub>3</sub> SS intensity ratios as a function of the number of carbons in the alkyl chain is shown in Fig. 3a. Intensity ratios ranging from 0.46  $\pm$  0.16 to 1.5  $\pm$  0.8 indicate that gauche defects were present in all five Quats solutions at the air-liquid interface. The graph suggests that the formation of gauche defects has a small dependence on increasing the chain length from C4 to C12. It is reported in the literature that any chain length from C16 to C22 forms a well-ordered monolayer [5]. Thus, SFG spectra from these ordered monolayers have minimal gauche defects [59]. Therefore, the gauche defects obtained from C4 -C12 Quats, which do not follow a particular trend, as a function of chain length can be due to factors such as the selected concentration to prepare Quats aqueous solutions and equilibration time.

The critical micelle concentration (CMC) plays an important role in how these surfactants adsorb and self-assemble at the airliquid interface. If CMC is not reached, a full monolayer or coverage will be difficult to confirm. Thus, the selection of the bulk concentration of these interfacial molecules can also be affected by the CMC level. Thus, if the selected concentration, at 8 mM, is below the CMC value for C4, C6, C8, C10, and C12, then we expect that the surfactants do not form a full monolayer at the air-liquid interface. Thus, this reflects the observation of gauche defects without any evident trend. However, although the CMC values for C4, C6, and C8 are difficult to determine [5], the surface tension values of the Quat solutions without salt were obtained using the Du Noüy ring method and plotted against concentration [60]. Five surface tension plots are provided in Fig. S3 in the Supporting Information. Fig. S3(a-c), plots for C4, C6, and C8 Quat aqueous solutions did not show more defined transitions to determine their CMC values even though higher concentrations greater than 8 mM were reached for C4, C6, and C8. As reported by Nguyen and group, less sharp transitions observed for C4, C6, and C8 solutions can be explained with the assumption that the surface excess/surface coverage of the topmost monolayer along with the formation of a submonolayer is unaffected. However, the surface tension value is consequently reduced due to the change in the conformation of the confined interfacial water molecules [61]. As the chain length was increased, the CMC values for both C10 and C12 are estimated to be  $\sim$ 5 mM and  $\sim$ 0.8 mM, respectively (Fig. S3(d) and Fig. S3(e)). The CMC values show that at C4, C6, and C8, the spectral profiles collected at 8 mM are all below their undefined CMC values. On the other hand, since the spectra acquired for both 8 mM C10 and C12 Quat molecules are above their estimated CMC values, the liquid surface is assumed to be completely covered with Quat molecules. However, as shown in Fig. 3(a), the CMC may not have a direct effect towards the number of gauche defects. The number of gauche defects increases with increasing alkyl chain length. Therefore, the formation of a well-ordered monolayer in relation to critical micelle concentration does not correlate with the increase in the number of gauche defects.

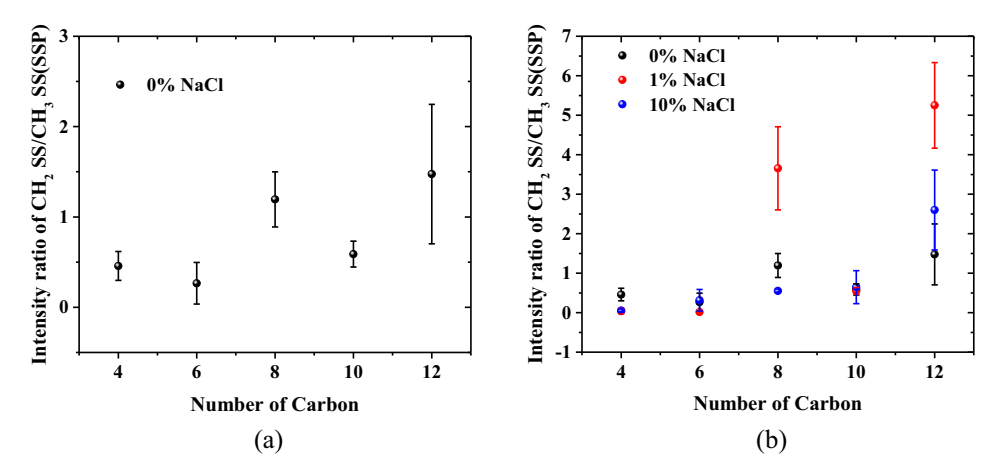


Fig. 3. The intensity ratio of CH<sub>2</sub> SS at ~2851 cm<sup>-1</sup> and CH<sub>3</sub> SS at ~2876 cm<sup>-1</sup> as a function of number of carbons in hydrophobic chain (a) 0% NaCl and (b) 0%, 1%, and 10% NaCl.

In addition, surface excess values were also determined from these surface tension plots to obtain a better idea of the monolayer coverage of these surfactants at the air-liquid interface. Therefore, to determine the surface excess concentrations of these surfactants, the Gibbs adsorption equation (Eq. (8)) can be applied [62–64].

$$\Gamma = -\frac{a}{nRT}\frac{\partial \gamma}{\partial a} = -\frac{c}{nRT}\frac{\Delta \gamma}{\Delta c} \tag{8}$$

where  $\Gamma$  is the surface excess concentration of solutes, a is the activity which can be replaced with c; the molar concentration of solutes,  $\gamma$  is the surface tension and n = 2 for ionic substances.  $\Delta \gamma$  =  $\gamma_{surfactant\ solution} - \gamma_{pure\ water}$  [64]. Table S2 available in the Supporting Information lists the surface excess values for each concentration of every chain length. A comparison plot between the surface excess values calculated from the 8 mM concentration of C4-C12 surfactants and intensity ratios (CH<sub>2</sub> SS/CH<sub>3</sub> SS) is presented in Fig. S4. The surface coverage or surface excess increases with increasing chain length at 8 mM concentration and starts to plateau at C10. The increasing number of surface coverage should have a relatively smaller number of gauche defects because of better packing between the alkyl chains. However, that is not the case for the observation obtained for C4, C6, and C8 Quat solutions. The surface excess/coverage for C10 and C12 aqueous solutions are 5.72  $\times$  $10^{14}$  and  $5.41\times 10^{14},$  respectively. The values are similar to each other. We suggest that these two concentrations lead to a saturation point or a full monolayer coverage. However, more points are needed to make that a valid assumption. Thus, a future study is considered and not yet regarded in the scope of this work. Comparing the C10 and C12 surface excess/coverage values versus the intensity ratios, with the assumption a full coverage is obtained and with an increased number of gauche defects, this scenario suggests that the interfacial molecules reached equilibrium and will only fluctuate due to other factors such as chemical nature of the surfactant, sample preparation, and equilibration time.

Another factor for the possible observation of gauche defects is that the 30-minute equilibration time or waiting time was not enough to form well-organized surfactants at the air-liquid interface at 8 mM solution. Therefore, we prepared 8 mM of C8 Quat surfactant in water and acquired ssp SFG spectra at 2900 cm<sup>-1</sup> IR center from 0, 0.5, 2, 4, to 6 h waiting time to monitor the change in the CH spectra profile and correlated it to a peak intensity difference between CH<sub>2</sub> SS and CH<sub>3</sub> SS (Fig. S5). The zero (0) time means the spectrum was collected right away after placing the C8 sample at the stage. As shown in the SI, the 0-time spectral profile still has

distinct peaks of the head group positioned at  $\sim$ 2972 cm<sup>-1</sup> and  $\sim$ 3065 cm<sup>-1</sup>. The ratio between the CH<sub>2</sub> SS and CH<sub>3</sub> SS slightly changes from 0-hr to 6-hr equilibration time as well, but there is no considerable effect towards the formation of gauche defects as a function of time. The results do not directly explain the nonlinear trend between the intensity ratio and the number of carbon atoms in the alkyl chain. A similar trend of nonlinear dependence between the number of gauche defects and length of the alkyl chain was also acquired as 1% and 10% of sodium chloride was introduced in the 8 mM Quat solutions (Fig. 3b). Since no trend was also obtained by adding salt, this means that increasing the ionic strength or the screening effect does not straightforwardly affect the number of gauche defects.

The overall observation obtained from the number of gauche defects and increasing alkyl chain can be supported by the explanation reported by Baldelli and Richmond groups wherein shorter chains usually possess less geometric gauche defects and less steric hindrance than longer alkyl chains [20,25]. These Quats are highly soluble in water and their critical micelle concentration (CMC) below C10 is challenging to determine using surface tension. So, the 8 mM concentration is not enough to achieve the highest surface concentration and confined conformational mobility with the nearest neighbors from C4 to C8 as explained by the surface excess calculation results [20,25]. Longer chain Quat compounds greater than C12 are found moderately soluble in water and thus not within the scope of this study.

3.3. Is the conformation of the interfacial water dependent on the length of the  $C_4$ - $C_{12}$  Quat surfactants?

Fig. 2 also shows that the SFG signal of OH stretches from 3000 to 3800 cm<sup>-1</sup>. As mentioned earlier, the two OH stretching modes are assigned to tetrahedrally and asymmetrically hydrogenbonded water molecular arrangements. Also, the free/dangling OH typically contributes to the SFG spectrum at the air-liquid interface where its peak is positioned at ~3650 cm<sup>-1</sup>. The fitting parameter results, for example, of 8 mM Quat solution ensure peak positions, peak assignments, and amplitudes which are available in Table S3 in the supporting information. The R-square value is also provided to show the goodness of the fit. In addition, all spectra were fitted with the corresponding standard deviation obtained from the three trials of the spectrum for every single point in the spectrum. The amplitude as a result of the fitting allows finding the relationship between the chain length, as determined by the increasing even number of carbons, and the SFG intensity. As the

two OH stretches changes as a function of the number of carbons, adding surfactants at the air-liquid interface affects the amount of the free OH molecules that are able to generate sufficient detected SFG photons. However, as shown in Fig. 2, the free OH peak is not prominent relative to other resonances because of several factors including the presence and concentration of surfactants. It is also known that higher concentrations lead to the disappearance of the dangling OH because more surfactants are occupying the surface [47,55,56]. The surface tension as affected by the concentration also affects the surface coverage. Surface coverage, on the other hand, affects the surface loading/activity of surfactants at the air-liquid interface which then reduces the contribution of the free OH. Also, the non-obvious presence of the free OH is also dependent on its total number of SFG counts compared to the SFG counts of the OH stretching mode positioned at 3182 cm<sup>-1</sup>. The SFG spectrum of an 8 mM C8 Quat centered at 3600 cm<sup>-1</sup> shows a relative count of ~75 of the free OH positioned at ~3650 cm<sup>-1</sup>. A future experiment is being considered to monitor the free OH as a function of the increasing concentration of the

Next, the spectral profile of the ssp polarization combination with a broad peak positioned at ~3182 cm<sup>-1</sup> indicates ordered water molecules at the air-liquid interface forming tetrahedral molecular arrangement in the presence of cationic Quat surfactants. The overall SF intensity of the OH stretch, as a result of the fitting process, increases from shorter alkyl chain to longer chain (C6-C12) in the ssp polarization, as shown in Fig. 4. However, the SFG intensity of the OH stretch in the C4 Quat surfactant has a higher relative value compared to the C6 molecule. A study performed by Singh and co-workers on the dependence of structural and orientation transformations of water with varying chain lengths of alcohol at the air-liquid interface reported that at the number of carbon atoms of linear chain alcohol from 1 to 3 (n < 4) does not affect the H-bonding capability and orientation of water molecules and the interface is unstable at n = 4 [65]. On the other hand, when n > 4, the interfacial water becomes more strongly H-bonded which was indicated by the maximum peak positioned at  $\sim$ 3200 cm<sup>-1</sup>. As shown in Fig. 4, C4 Ouat behaves differently from C6-C12 surfactants. After waiting for 30 min or more and performing the experiment multiple times, C4 alkyl chain length adsorbs similarly at the air-liquid interface when compared to longer chain length (C8-C12). This behavior indicates a structural and/or orientational transition of the interfacial water at the surfactant-water interface which was the same observation obtained by Singh and colleagues [65]. Also, according to Nguyen and colleagues, by connecting our surface tension and SFG results, the formation of an immersed surfactant bilayer results in an unaf-

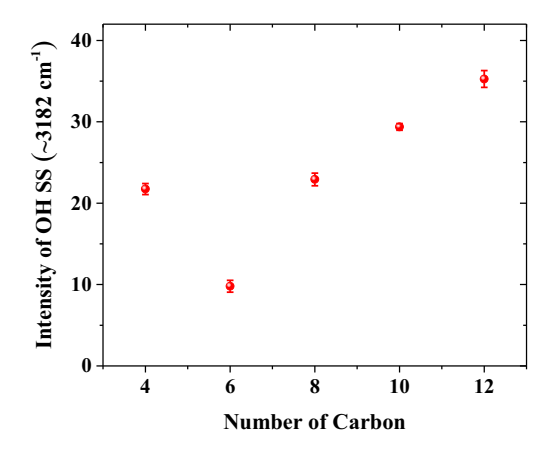


**Fig. 4.** The intensity of OH SS at  $\sim$ 3182 cm<sup>-1</sup> as a function of the number of carbons in the hydrophobic chain (0% NaCl).

fected topmost surfactant monolayer and a reduction of surface tension value when the confined interfacial molecules rearranged [61]. The spectral profile of the alkyl chain of the C4 molecule remains similar to other chain lengths, while in the OH region showed the formation of ordered hydrogen-bonded water molecules. In addition, the transition is associated with the hydrophobic size of the chain relative to the size of the cationic headgroup. To support our explanations, we also check the pH of all solutions (C4–C12) without salt to make sure that there is no pH dependence. The pH values for 8 mM Quat solutions are available in Table S4 of the Supporting Information. Since the pH values for each Quat aqueous solution are similar, the pH will globally affect the behavior of all solutions similarly. The pH value of ~5.54 obtains an acid dissociation constant ( $K_0$ ) of ~1.19 × 10<sup>-09</sup>.

Next, as shown in Fig. S6, 1 mM concentration of alkyltetramethylammonium bromide (ATAB) surfactants with alkyl chain lengths of n = 4 to n = 12 (4, 6, 8, 10, 12) solutions were prepared. This experiment was performed to check whether the headgroup affects the arrangement of water molecules at the air-liquid interface, especially for the C4 surfactant. However, after analysis, the ssp SFG spectrum of the C4 TAB solution did not show any evident vibrational signatures from -CH<sub>3</sub>, -CH<sub>2</sub>, or the -N-CH<sub>3</sub> functional groups (Fig. S6). Therefore, as a result, the structural changes of interfacial water molecules observed for the C4 surfactant can also be dependent on the chemical nature of the cationic headgroup. Another possible reason for this observation could also be because the concentration of the C4 TAB solution is not sufficient to cause the surface activity of these C4 TAB molecules at the air-liquid interface. This means that the surface coverage of an 8 mM Quat aqueous solution is not equivalent to the surface coverage of a 1 mM C4 TAB aqueous solution. To further investigate the concern over the coverage, surface tension measurements were performed for both C4 Quat and C4 TAB solutions with a concentration range from 0 to 120 mM. This enables the comparison of the surface tension values to find the matching concentration of the 8 mM C4 Quat from the plot of C4 TAB (Fig. S7). The equivalent concentration was found to be ~102 mM of C4 TAB solution which will have similar surface coverage with 8 mM of C4 Ouat solution. Then the ssp SFG spectra of 8 mM C4 Quat and 102 mM C4 TAB solution were acquired. Fig. 5 shows the spectral profiles of the two solutions. The OH stretch vibrational mode positioned at ~3182 cm<sup>-1</sup> is evident in the ssp spectrum of the 8 mM C4 Quat solution while not clearly present in the ssp SFG spectrum of ~102 mM C4 TAB solution. The possible reasons for these observations are (1) the headgroup has a role in the organization of the water molecules at the air-liquid interface and/or (2) the approach of finding the matching concentration for 8 mM C4 Quat solution using the surface tension measurement does not define a 1:1 correlation with the SFG measurements. Looking closely at Fig. 5b, the SSP spectrum of the 8 mM C4 Quat has the vibrational signature of the Quat headgroup positioned at 3068 cm<sup>-1</sup>. This peak is a CH aromatic stretch of the benzyl group. The comparison of ssp spectra (Fig. S8) of the C4 Quat with 0%, 1%, and 10% shows that the presence of 1% and 10% salt has effectively reduced the spectral interference from water molecules and has only emphasized the contribution of the headgroup at ~3068 cm<sup>-1</sup>. Therefore, the surface activity of the C4 Quat is also assisted by the headgroup's existing interaction and overall conformation in aqueous solution. In regard to the 1:1 correlation of the Ouat and TAB surfactants concentration for surface coverage equivalence, finding its absolute correlation will require further investigation which will be performed in our future studies.

This study also supports earlier findings that the SFG signal of the OH stretches in the 3000–3800 cm<sup>-1</sup> region is enhanced in the presence of surfactants [18,47,50,66]. The adsorption of surfactants at the air-water interface creates a large electrostatic field

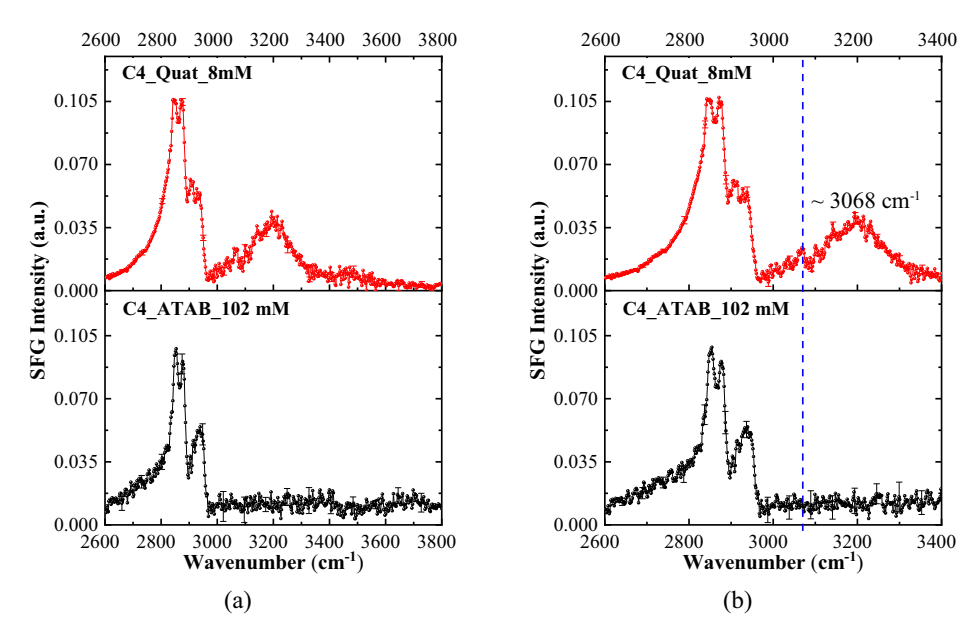


Fig. 5. (a) ssp SFG spectra of both 8 mM C4 Quat and C4 TAB aqueous solutions from  $2600 - 3800 \text{ cm}^{-1}$  and (b) ssp SFG spectra from  $2600 \text{ to } 3400 \text{ cm}^{-1}$  to emphasize the peak positioned at  $\sim 3068 \text{ cm}^{-1}$ .

and interfacial water molecules orient themselves relative to the surface charge of surfactants which enhances the SFG signal at the OH region. According to the flip-flop model of interfacial water molecules suggested by Tahara and co-workers, the oxygen of water molecules is pointed up to the positively charged surface. On the other hand, the hydrogen of water molecules is pointed up to the negatively charged surface [47]. Using the flip-flop model of the charged surfactant-aqueous interface, the cationic Quat compound orients OH bands of interfacial water molecules with their hydrogen pointing down from the positive charge of the Quat headgroup. This study also supports the recent findings by Singh and co-workers [65] from which the long hydrophobic alkyl chains of alcohol affect interfacial water differently than the shorter chain length alcohol. However, according to their findings, the shorter chain length (n = 1-3) of alcohol does not affect the hydrogen bonding and the orientation of the interfacial water substantially and the interface is quite unstable for n = 4, as stated earlier [65]. Another group found that the adsorption of short-chain alcohol at the air-water interface is similar to the classical surfactants [67]. Critical aggregation concentration (CAC) of alcohol and the critical micelle concentration (CMC) of surfactants were considered for comparisons. The alcohols and surfactants possess linear dependence of Gibbs standard free energy of their adsorption at the air-water interface as a function of hydrophobic chain length [67]. Therefore, as shown in Fig. 4, the OH stretch intensity drops (~3182 cm<sup>-1</sup>) from C4 to C6 can also be explained by which the interface becomes unstable because of the reduced interaction between these shorter chain length surfactants and water molecules. Thus, resulting in more randomly oriented interfacial molecules affecting the overall SFG signal of the C6 surfactant in water. In addition, the major increase of OH stretch intensity for the longer chains is direct evidence of the effect of alkyl chain length on the orientation of the interfacial water molecules and increased hydrophobic interaction between the chains. In a bulk study, Raman multivariate curve resolution (Raman-MCR) spectroscopy showed that longer chain length surfactants form micelle in the bulk and the interfacial water molecules can penetrate much deeper into the hydrophobic core of the micelle. This observation has resulted in more ordered interfacial water molecules [68].

3.4. How do the conformations of both the chain and the water molecules change with increasing ionic strength?

The effects of salts in aqueous solutions play an important role in the aggregation behaviors of ionic surfactants [69]. The addition of salt reduces the electrostatic repulsion between the cationic headgroups, which results in their much closer assembly to each other at the air-liquid interface. This also leads to the reduction of the CMC value as well [57]. As shown in Figs. 6 and 7, the addition of 1% and 10% salt (see Table S5 for the respective ionic strengths) in 8 mM aqueous solutions of C4, C6, C8, C10, and C12 Ouats affected the conformation of the chain length. Looking closely at the results of both ssp and ppp polarization combinations, the changes in the intensity and spectral profiles of Quat molecules from C4 to C12 are contributions from the interactions existing between non-polar hydrocarbon (HC) chains and polar head group - water molecules due to the increasing presence of salt. The SFG spectra from a 1% NaCl solution show the signal from the chain (CH<sub>2</sub> and CH<sub>3</sub> groups), the head group (-N-CH<sub>3</sub> and CH aromatic groups) and —OH SS of water molecules (Fig. 6).

Yet, with the increasing number of carbons, a decrease in the OH SS (at ~3182 cm<sup>-1</sup>) is observed relative to the intensity of the −N−CH<sub>3</sub> group while the OH SS at ~3384 cm<sup>-1</sup> seems to be unperturbed. For 1% (0.17 M) salt (Table S5), it is difficult to obtain a clear trend for the CH spectral profile, however, the vibrational signature from the headgroup becomes more distinct as the signal from the OH stretch decreases. Also, the weakly-bonded H<sub>2</sub>O molecules become more prominent relative to the strongly-bonded H<sub>2</sub>O molecules. Interestingly, the changes in the spectral profiles of C4, C6, C8, C10, and C12 in the presence of 10% salt (1.7 M) are more noticeable (Fig. 7). SFG signal from interactions between the alkyl chains and arrangement of the head group is still noticeable from C4- C12 Quat surfactants. However, the SFG signal from the strongly-bonded water molecules positioned at ~3182 cm<sup>-1</sup> had decreased when compared to the results obtained from 8 mM Quat aqueous solution with 1% NaCl. Thus, a lesser contribution was evident from the constructive interference created between the OH and CH vibrational modes. The CH spectral profiles show no trend, yet carefully analyzing the distinct C4 ssp and ppp spectra, the intensity ratio between CH<sub>2</sub> SS and CH<sub>3</sub> SS

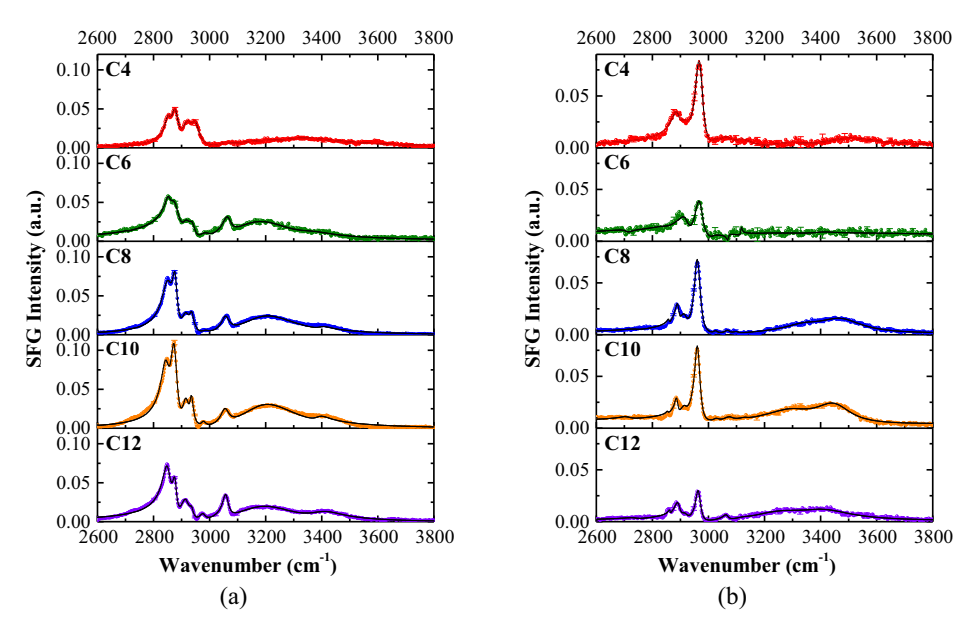


Fig. 6. Fitted SFG spectra of 8 mM C4, C6, C8, C10, and C12 in water (1% NaCl) at (a) ssp and (b) ppp polarization combinations.

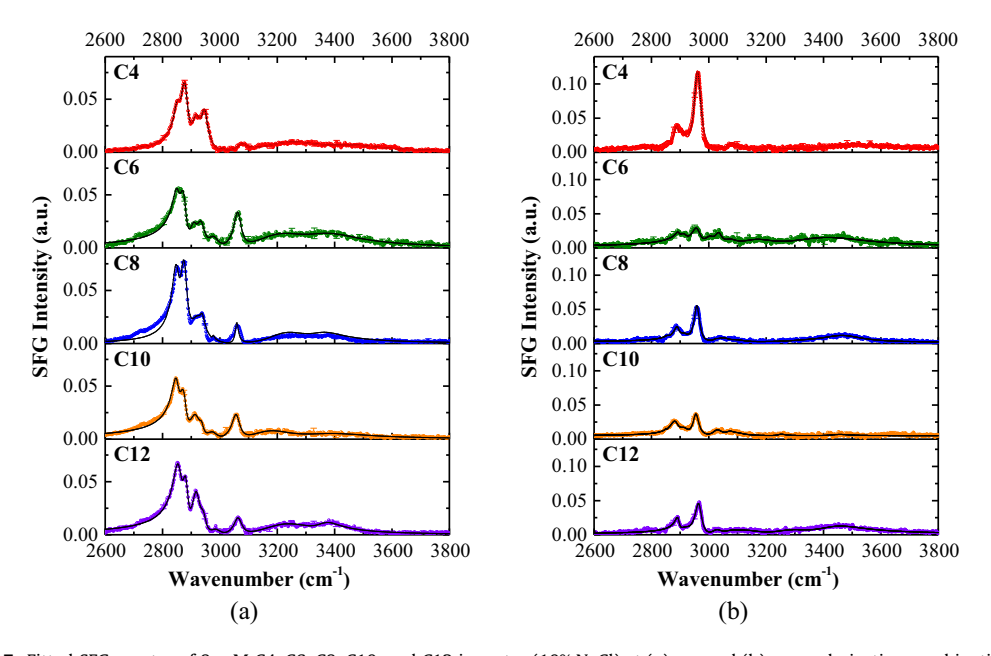
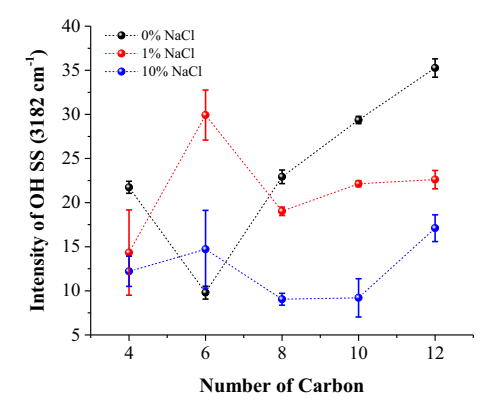


Fig. 7. Fitted SFG spectra of 8 mM C4, C6, C8, C10, and C12 in water (10% NaCl) at (a) ssp and (b) ppp polarization combinations.

decreases. This means less number of gauche defects with 1% NaCl. In addition, we also calculated the tilt angle [28] for the terminal methyl group of C4 and found the value to be  $39^{\circ} \pm 27^{\circ}$  for 0% salt and  $45^{\circ} \pm 84^{\circ}$  for 1% salt from the surface normal. The tilt angle of the terminal methyl group of the Quat surfactant series was determined by calculating the intensity ratio between the CH<sub>3</sub> SS and CH<sub>3</sub> AS from the fitted ppp spectra and comparing it with the simulated curve. The ppp polarization combination was chosen over the ssp polarization combination to avoid convolutions of the spectral interference between CH<sub>3</sub> SS and Fermi interactions and the spectral interference CH and OH region [28,50]. The approach to generating the simulated curve was reported in previous studies and the parameters (Table S6) of the simulated SFG curve are listed in the Supporting Information [38,60]. The parameters considered for the SFG simulation curve, the simulated curve, the calculated

tilt angle values, and  $R^2$  values for different chain lengths and salt concentrations are reported in Table S6, Fig. S9, and Table S7, and Table S8, respectively.

This observation regarding gauche defects is due to the addition of salt which reduces the electrostatic repulsion between the head groups, allowing the close packing of the surfactants at the airliquid interface. Therefore, more surfactants are adsorbed at the interface which facilitates the decrease in its surface tension as well as reduction of the electrostatic field. The hydrophobic interactions between alkyl chains arranged the polar head group in an orderly manner to each other. At the same time, the OH group contribution has been reduced affecting the arrangement of the water molecules in the double-layer region via the formation of hydrogen bonds along with some contributions from the intramolecular interaction as a result of the vibronic coupling of the OH SS with



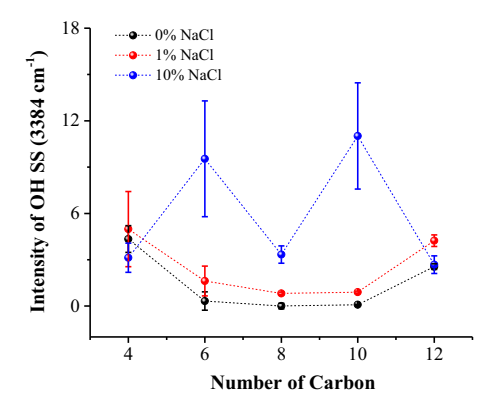


Fig. 8. The plot of the intensity of OH SS at ~3182 cm<sup>-1</sup> and ~3384 cm<sup>-1</sup> as a function of the number of carbon atoms in the alkyl chain at different NaCl concentrations.

the bending mode [19,29]. To summarize, Fig. 8 shows the graph with OH SS at  $\sim$ 3182 cm<sup>-1</sup> and  $\sim$ 3384 cm<sup>-1</sup> from 0%, 1%, and 10% as a function of increasing chain length.

However, the overall effect introduced by salt in the solutions of increasing chain length does not provide a clear trend. Therefore, in Fig. S10, the OH stretch was plotted as a function of 0, 1, and 10% salt concentration for C4-C12 surfactants. There is no clear trend for C6 Quat because, at 0%, the OH intensity is low and increases at 1% and then decreases again for 10%. However, a decreasing trend of the OH intensity at ~3182 cm<sup>-1</sup> is observed from C4, C8, C10, to C12. Consequently, the OH stretch signal at ~3182 cm<sup>-1</sup> decreases as we increased the salt concentration from 0, 1% to 10%. The implication of can be very well-correlated to the affected contributions of the second-order nonlinear susceptibility,  $\chi^{(2)}$ , and the third-order optical properties of the bulk water,  $\chi^{(3)}$ , in view of the overall SFG signal from a charged interface and decreasing OH stretch interference [29]. The C6 Quat molecule in water was characterized multiple times to ensure the repeatability of the spectral results. In such a case, we must find a reason behind the C6 response to increasing salt concentration upon monitoring the OH stretch at ~3182 cm<sup>-1</sup>. The hydrophobic size of the C4 Quat compound may have affected the

OH stretch intensity, which resulted in a structural transformation of the interfacial water and that is why its OH spectra profile is similar to C8, C10, and C12. On the other hand, the  $\rm H_2O$  molecules are not strongly hydrogen-bonded in the aqueous solution of C6 Quat molecules with 0% salt. At 1% salt, an increase in the SFG signal was obtained at ~3182 cm $^{-1}$ , which indicated that the  $\rm H_2O$  molecules at the interface and the double layer are arranged more orderly. Then, a sudden decrease for the OH SS vibrational mode SFG signal was observed at 10% salt which resulted in a decrease in the order between the arranged  $\rm H_2O$  molecules.

In the case of the shortest chain length (C4), our results indicated a more ordered monolayer was achieved by increasing the NaCl concentration to 1.70 M (Fig. S8). This increased contribution from the terminal methyl symmetric suggested a considerable effect on the ordering of short-chain surfactants due to ionic strength when compared to the presence of no salt and  $\sim$ 1.70 M salt. In addition, increasing the ionic strength results in a decrease in the OH band of the interfacial water at a positively charged interface [31]. As shown in the C4 spectra from 0%, 1%, and 10% salt content (Fig. S8), the OH band signal is relatively reduced where water ordering is random; yet has a more ordered hydrocarbon chain.

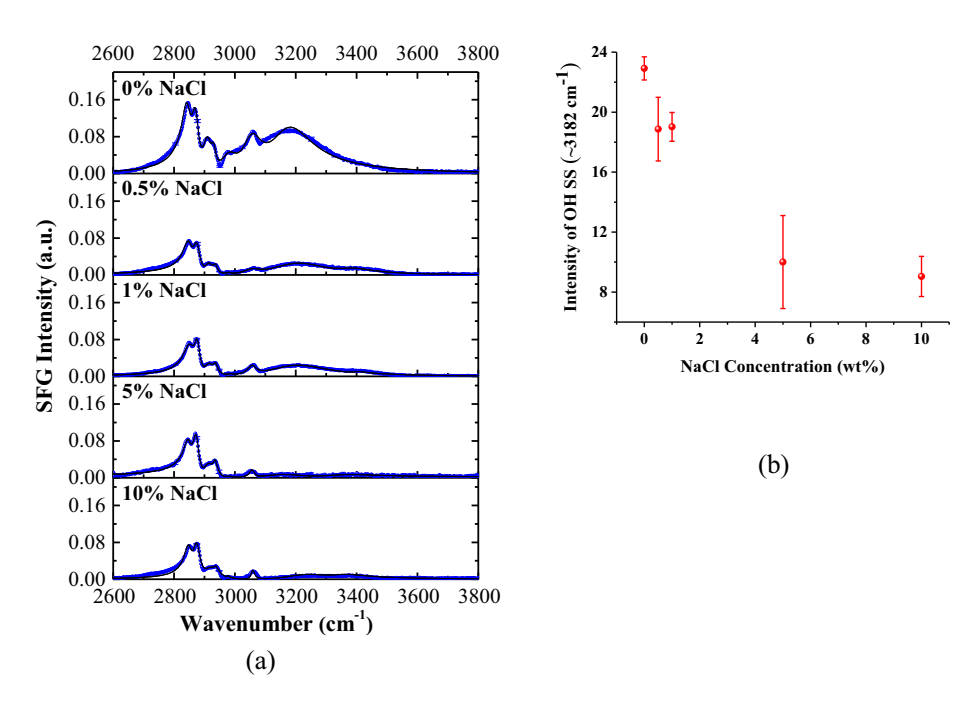


Fig. 9. (a) Fitted SFG spectra of 8 mM C8 in water with 0%, 0.5%, 1%, 5%, and 10% NaCl at ssp Polarization combinations and (b) the intensity of OH SS at ~3182 cm<sup>-1</sup> as a function of NaCl concentration.

3.5. How does increasing ionic strength specifically affects the OH band?

In this discussion, 8 mM C8 Quat molecule was prepared with 0%, 0.5%, 1.0%, 5%, and 10% salt, which has equivalent/corresponding ionic strength values listed in Table S5 available in the Supporting Information. Fig. 9a presents ssp spectra for the C8 Quat molecules and Fig. 9b plots the intensity of the OH band positioned at ~3182 cm<sup>-1</sup>. The ppp spectra are shown in the Supporting Information (Fig. S11). The OH band decreases with increasing ionic strength. This observation, as noted earlier, is because of the charge screening effect as a result of increasing the salt concentration. The Debye screening length is reduced which in effect also affects the volume of the noncentrosymmetric region at the air-liquid interface resulting in a reduced SFG signal [30]. Also, a decrease in the overall SFG signal in the CH region is also observed after the addition of salt but the spectral profile is structurally invariant [29,70]. To summarize, the reduction in both the CH and OH signal is in line with the contributions coming from the second-order resonant susceptibility  $(\chi^{(2)})$  and the third-order optical properties of the bulk water ( $\chi^{(3)}$ ). The  $\chi^{(3)}$  contribution can be qualitatively determined from the intensity difference between varied salt concentrations; a method developed by Geiger and coworkers [29]. The addition of 0.5% and 5% of NaCl relatively shows the gradual decrease in the OH SS at  $\sim$ 3182 cm<sup>-1</sup>.

In addition to the explanation using the screening effect, the intensity of the OH bands of the interfacial water at a cationic surfactant interface decreases with increasing salt concentration can also be explained by the counterion effect [26,31,71]. Increasing salt concentration dramatically changes the interfacial hydrogen bonding as shown by Doughty and co-workers. Anion can adsorb into the Quat/water interface and perturb the hydrogen-bonding networks [71]. Similar studies from Tahara and coworkers using CTAB and sodium halides show that the OH band intensity of interfacial water decreases in the order of the Hofmeister series. High salt concentration generates Helmholtz electric double layers in which counterions are present near to the interface region. The interfacial water molecules are restricted in between the charged monolayer and counterions and orient themselves by the electric field. The OH band intensity was found to have decreasing order with increasing size of the halide ions. The peak frequency shifting to a higher wavenumber indicates the hydrogen bond is weakened at CTA<sup>+</sup>/Cl<sup>-</sup> interfaces [31]. The similar changes in OH band intensity with added salt was also observed in our work. In Fig. S11, as the salt concentration increases from 0%, 0.5%, 1%, 5%, and 10%, the overall OH bands intensity decreases and the intensity of OH and at  $\sim\!\!3182~\text{cm}^{-1}$  becomes less prominent and the intensity of OH band at ~3384 cm<sup>-1</sup> becomes more noticeable. Thus, the observation of the peak frequency shifting to a higher wavenumber can also be explained that due to the presence of Cl<sup>-</sup> counterions at the Quat/water interface, the interfacial hydrogen-bonding network is disturbed. At 5% and 10% salt, the OH band has almost vanished indicating that the number of oriented water molecules present in the Quat/Cl<sup>-</sup> interfaces has decreased [31,71].

#### 4. Conclusion

The chain length dependence of C4, C6, C8, C10, and C12 Quat surfactants have been successfully studied with different ionic strengths at the air-water interfaces by SFG. From the SFG spectra, we can conclude that this series of surfactants retains surface activity with a considerable number of gauche defects even at short alkyl chain lengths. The previous studies focusing on chain length and ionic strength reported their observations about gauche defects of alkyl chain [16,17,24,25,65] and conformational changes

of interfacial water independently [18,19,28,30,31,65]. The number of gauche defects decreases with increasing chain length was observed at air-solid and air-liquid interfaces [23,24] and decreasing trend of gauche defects was also reported with decreasing chain length at the liquid-liquid interface [25]. On the other hand, the ionic strength dependence shows that the interfacial water molecules become less ordered with increasing salt concentration [18,28–30]. In this work, we reported the combined effect of chain length and ionic strength variations on the conformational changes of surfactant-water interfaces. This research provides several new findings: (1) No clear trend was obtained for the number of gauche defects as a function of increasing chain length from C4 to C12. Less number of gauche defects were observed for shorter chain lengths while an increasing number of gauche defects were observed for longer carbon chains, (2) The number of gauche defects decreases for the shortest chain surfactant (C4) as a function of ionic strength, (3) Increasing the alkyl chain length (C6, C8, C10, and C12) results to more ordered interfacial water molecules. The SFG intensity of the OH SS vibrational mode of C8 Quat at 3182 cm<sup>-1</sup> in water has decreased with increasing ionic strength, (4) At a similar surface coverage, C4 Quat showed SFG signal from OH SS vibrational modes as a signature for more ordered water molecules at the air-liquid interfaces compared to a C4 TAB surfactant. While no evident SFG signal from the OH vibrational mode was observed for C4 TAB surfactant. This result showcases the role of the chemical nature of headgroup towards the formation of tetrahedrally arranged water molecules at the air-liquid interface in the presence of a shorter alkyl chain, and (5) The hydrogen bonding formation between water molecules was affected and enhanced in the presence of a C4 Quat surfactant. On the other hand, a recent study of alcohol with varying alkyl length reported that the interface is unstable with C4 alcohol [65]. These findings support previous studies on chain length [16,17,24,25,65] and ionic strength [18,19,28,30,31]. This work provides an evidence to consider effective number of carbon on alkyl chain at different ionic strength, self-assembly of surfactants with different headgroup, and conformational changes of interfacial water molecules undergone by increasing chain length and ionic strength which leads to our future work on self-assembly of surfactants at liquid-metal interface. In addition, we presented the adsorption behavior of a series of highly water-soluble short-chain surfactants of limited CMCs which will benefit in designing new surfactants for a specific environment in corrosion inhibition [18-23], fabric softeners, interfacial processes, self-assembly, micellization, and other related fields [5,72-74].

# **CRediT authorship contribution statement**

**Md. Rubel Khan:** Investigation, Validation, Formal analysis, Writing - original draft, Visualization. **Uvinduni I. Premadasa:** Validation, Investigation, Writing - review & editing. **Katherine Leslee A. Cimatu:** Conceptualization, Methodology, Validation, Writing - review & editing, Supervision.

#### **Declaration of Competing Interest**

The authors declare that they have no known competing financial interests or personal relationships that could have appeared to influence the work reported in this paper.

### Acknowledgment

The authors acknowledge with sincere gratitude Drs. David Young, Marc Singer, Srdjan Nesic, Sumit Sharma and graduate student, Negar Moradighadi from the Institute of Corrosion and Multiphase Technology (ICMT) in the Department of Chemical and Biomolecular Engineering at Ohio University for fruitful discussions. This work is supported by a grant from the National Science Foundation (NSF; grant CBET-1705817). The authors would like to thank NSF (grants CHE-0947031 and CHE-1338000) for the acquisition of the femtosecond laser and nuclear magnetic spectrometer. Additionally, the authors are grateful to the Department of Chemistry and Biochemistry, the College of Arts and Sciences, the Vice President for Research and the Nanoscale and Quantum Phenomena Institute for financial support.

## Appendix A. Supplementary material

The Supporting Information is available free of charge on the Elsevier Publications website via the Internet at <a href="https://www.elsevier.com">https://www.elsevier.com</a>. The purity of synthesized Quats, the surface tension of Quats in water, surface excess concentrations, pH values and ionic strengths of 8 mM Quat solutions, additional SFG spectra, fitting results, simulated SFG curves, and parameters for generating the simulated SFG curves for the orientational analysis. (PDF). Supplementary data to this article can be found online at <a href="https://doi.org/10.1016/j.jcis.2020.02.056">https://doi.org/10.1016/j.jcis.2020.02.056</a>.

#### References

- [1] M.A. Migahed, A.M. Al-Sabagh, Beneficial role of surfactants as corrosion inhibitors in petroleum industry: a review article, Chem. Eng. Commun. 196 (9) (2009) 1054–1075.
- [2] Y. Zhu, M.L. FreeM, Effects of surfactant aggregation and adsorption on steel corrosion inhibition in salt solution, Polymer Sciences (2015).
- [3] D.E. Gragson, G.L. Richmond, Probing the structure of water molecules at an oil/water interface in the presence of a charged soluble surfactant through isotopic dilution studies, J. Phys. Chem. B 102 (3) (1998) 569–576.
- [4] C. Li, S. Richter, S. Nešići, How do inhibitors mitigate corrosion in oil-water two-phase flow beyond lowering the corrosion rate?, Corrosion 70 (9) (2014) 958–966.
- [5] I.J. Lin, B.M. Moudgil, P. Somasundaran, Estimation of the effective number of— CH<sub>2</sub>-groups in long-chain surface active agents, Colloid Polym. Sci. 252 (5) (1974) 407–414.
- [6] M. Finšgar, J. Jackson, Application of corrosion inhibitors for steels in acidic media for the oil and gas industry: a review. Corros. Sci. 86 (2014) 17–41.
- [7] M.B. Kermani, D. Harrop, The impact of corrosion on oil and gas industry, SPE Prod. Facil. 11 (03) (1996) 186–190.
- [8] A.J. McMahon, The mechanism of action of an oleic imidazoline based corrosion inhibitor for oilfield use, Colloids Surf. 59 (1991) 187–208.
- [9] L.T. Popoola, A.S. Grema, G.K. Latinwo, B. Gutti, A.S. Balogun, Corrosion problems during oil and gas production and its mitigation, Int. J. Ind. Chem. 4 (1) (2013) 35.
- [10] J. Cruz, R. Martinez, J. Genesca, E. Garcia-Ochoa, Experimental and theoretical study of 1-(2-ethylamino)-2-methylimidazoline as an inhibitor of carbon steel corrosion in acid media, J. Electroanal. Chem. 566 (1) (2004) 111–121.
- [11] Y.-J. Tan, S. Bailey, B. Kinsella, An investigation of the formation and destruction of corrosion inhibitor films using electrochemical impedance spectroscopy (EIS), Corros. Sci. 38 (9) (1996) 1545–1561.
- [12] C.K. Nmai, S.A. Farrington, G. Bobroski, Organic-based corrosion-inhibiting admixture for reinforced concrete. Concr. Int. 14 (4) (1992) 45–51
- admixture for reinforced concrete, Concr. Int. 14 (4) (1992) 45–51.

  [13] I. Jevremović, M. Singer, S. Nešić, V. Mišković-Stanković, Inhibition properties of self-assembled corrosion inhibitor talloil diethylenetriamine imidazoline for mild steel corrosion in chloride solution saturated with carbon dioxide, Corros. Sci. 77 (2013) 265–272.
- [14] M. Knag, J. Sjöblom, G. Øye, E. Gulbrandsen, A quartz crystal microbalance study of the adsorption of quaternary ammonium derivates on iron and cementite, Colloids Surf., A 250 (1–3) (2004) 269–278.
- [15] Y. Tang, X. Yang, W. Yang, R. Wan, Y. Chen, X. Yin, A preliminary investigation of corrosion inhibition of mild steel in 0.5 M H<sub>2</sub>SO<sub>4</sub> by 2-amino-5-(n-pyridyl)-1, 3, 4-thiadiazole: polarization, EIS and molecular dynamics simulations, Corros. Sci. 52 (5) (2010) 1801–1808.
- [16] G.R. Bell, C.D. Bain, R.N. Ward, Sum-frequency vibrational spectroscopy of soluble surfactants at the air/water interface, J. Chem. Soc., Faraday Trans. 92 (4) (1996) 515–523.
- [17] K. Cimatu, H.J. Moore, D. Barriet, P. Chinwangso, T.R. Lee, S. Baldelli, Sum Frequency generation imaging microscopy of patterned self-assembled monolayers with terminal -CH<sub>3</sub>,-OCH<sub>3</sub>,-CF<sub>2</sub>CF<sub>3</sub>,-C=C,-phenyl, and -cyclopropyl groups, J. Phys. Chem. C 112 (37) (2008) 14529–14537.
- [18] W. Sung, Z. Avazbaeva, D. Kim, Salt promotes protonation of amine groups at air/water interface, J. Phys. Chem. Lett. 8 (15) (2017) 3601–3606.

- [19] D.E. Gragson, B.M. McCarty, G.L. Richmond, Surfactant/water interactions at the air/water interface probed by vibrational sum frequency generation, J. Phys. Chem. Lett. 100 (34) (1996) 14272–14275.
- [20] C. Aliaga, G.A. Baker, S. Baldelli, Sum frequency generation studies of ammonium and pyrrolidinium ionic liquids based on the bistrifluoromethanesulfonimide anion, J. Phys. Chem. B 112 (6) (2008) 1676– 1684.
- [21] K.C. Jena, P.A. Covert, D.K. Hore, The effect of salt on the water structure at a charged solid surface: differentiating second-and third-order nonlinear contributions, J. Phys. Chem. Lett. 2 (9) (2011) 1056–1061.
- [22] A.A. Shahir, K. Khristov, K.T. Nguyen, A.V. Nguyen, E. Mileva, Combined sum frequency generation and thin liquid film study of the specific effect of monovalent cations on the interfacial water structure, Langmuir 34 (23) (2018) 6844-6855.
- [23] C. Reitböck, E. Głowacki, D. Stifter, Sum-frequency generation vibrational spectroscopy investigations of phosphonic acids on anodic aluminum oxide films, Appl. Spectrosc. 72 (5) (2018) 725–730.
- [24] J.C. Conboy, M.C. Messmer, G.L. Richmond, Investigation of surfactant conformation and order at the liquid–liquid interface by total internal reflection sum-frequency vibrational spectroscopy, J. Phys. Chem. 100 (18) (1996) 7617–7622.
- [25] J.C. Conboy, M.C. Messmer, G.L. Richmond, Effect of alkyl chain length on the conformation and order of simple ionic surfactants adsorbed at the D2O/CCI4 interface as studied by sum-frequency vibrational spectroscopy, Langmuir 14 (23) (1998) 6722–6727.
- [26] D. Liu, G. Ma, L.M. Levering, H.C. Allen, Vibrational spectroscopy of aqueous sodium halide solutions and air—liquid interfaces: observation of increased interfacial depth, J. Phys. Chem. B 108 (7) (2004) 2252–2260.
- [27] T. limori, T. Iwahashi, K. Kanai, K. Seki, J. Sung, D. Kim, H.-O. Hamaguchi, Y. Ouchi, Local structure at the air/liquid interface of room-temperature ionic liquids probed by infrared—visible sum frequency generation vibrational spectroscopy: 1-alkyl-3-methylimidazolium tetrafluoroborates, J. Phys. Chem. B 111 (18) (2007) 4860–4866.
- [28] U.I. Premadasa, N. Moradighadi, K. Kotturi, J. Nonkumwong, M.R. Khan, M. Singer, E. Masson, K.L.A. Cimatu, solvent isotopic effects on a surfactant headgroup at the air-liquid interface, J. Phys. Chem. C 122 (28) (2018) 16079–16085
- [29] M. Dogangun, P.E. Ohno, D. Liang, A.C. McGeachy, A.G. Be, N. Dalchand, T. Li, Q. Cui, F.M. Geiger, Hydrogen-bond networks near supported lipid bilayers from vibrational sum frequency generation experiments and atomistic simulations, J. Phys. Chem. B 122 (18) (2018) 4870–4879.
- [30] K.C. Jena, D.K. Hore, Variation of ionic strength reveals the interfacial water structure at a charged mineral surface, J. Phys. Chem. C 113 (34) (2009) 15364–15372.
- [31] S. Nihonyanagi, S. Yamaguchi, T. Tahara, Counterion effect on interfacial water at charged interfaces and its relevance to the Hofmeister series, J. Am. Chem. Soc. 136 (17) (2014) 6155–6158.
- [32] K.A. Cimatu, S.C. Chan, J.H. Jang, K. Hafer, Preferential organization of methacrylate monomers and polymer thin films at the air interface using femtosecond sum frequency generation spectroscopy, J. Phys. Chem. C 119 (45) (2015) 25327–25339.
- [33] A.G. Lambert, P.B. Davies, D.J. Neivandt, Implementing the theory of sum frequency generation vibrational spectroscopy: a tutorial review, Appl. Spectrosc. Rev. 40 (2) (2005) 103–145.
- [34] J. Kim, G.A. Somorjai, Molecular packing of lysozyme, fibrinogen, and bovine serum albumin on hydrophilic and hydrophobic surfaces studied by infrared—visible sum frequency generation and fluorescence microscopy, J. Am. Chem. Soc. 125 (10) (2003) 3150–3158.
- [35] M. Maroncelli, H.L. Strauss, R.G. Snyder, The distribution of conformational disorder in the high-temperature phases of the crystalline n-alkanes, J. Chem. Phys. 82 (6) (1985) 2811–2824.
- [36] H.-F. Wang, W. Gan, R. Lu, Y. Rao, B.-H. Wu, Quantitative spectral and orientational analysis in surface sum frequency generation vibrational spectroscopy (SFG-VS), Int. Rev. Phys. Chem. 24 (2) (2005) 191–256.
- [37] H.Z. Sommer, H.I. Lipp, L.L. Jackson, Alkylation of amines General exhaustive alkylation method for the synthesis of quaternary ammonium compounds, J. Org. Chem. 36 (6) (1971) 824–828.
- [38] S.C. Chan, J.H. Jang, K.A. Cimatu, Orientational analysis of interfacial molecular groups of a 2-methoxyethyl methacrylate monomer using femtosecond sum frequency generation spectroscopy, J. Phys. Chem. C 120 (51) (2016) 29358–29373.
- [39] J.C. Duplan, L. Mahi, J.L. Brunet, NMR determination of the equilibrium constant for the liquid H2O–D2O mixture, Chem. Phys. Lett. 413 (4–6) (2005) 400–403
- [40] A.D. Quast, N.C. Wilde, S.S. Matthews, S.T. Maughan, S.L. Castle, J.E. Patterson, Improved assignment of vibrational modes in sum-frequency spectra in the CH stretch region for surface-bound C18 alkylsilanes, Vib. Spectrosc. 61 (2012) 17–24.
- [41] L.J. Richter, T.P. Petralli-Mallow, J.C. Stephenson, Vibrationally resolved sumfrequency generation with broad-bandwidth infrared pulses, Opt. Lett. 23 (20) (1998) 1594–1596.
- [42] D. Verreault, V. Kurz, C. Howell, P. Koelsch, Sample cells for probing solid/liquid interfaces with broadband sum-frequency-generation spectroscopy, Rev. Sci. Instrum. 81 (6) (2010) 063111.

- [43] E. Tyrode, M.W. Rutland, C.D. Bain, Adsorption of CTAB on hydrophilic silica studied by linear and nonlinear optical spectroscopy, J. Am. Chem. Soc. 130 (51) (2008) 17434–17445.
- [44] K.T. Nguyen, A.V. Nguyen, Suppressing interfacial water signals to assist the peak assignment of the N+–H stretching mode in sum frequency generation vibrational spectroscopy, PCCP 17 (43) (2015) 28534–28538.
- [45] C. Dutta, A. Svirida, M. Mammetkuliyev, M. Rukhadze, A.V. Benderskii, Insight into water structure at the surfactant surfaces and in microemulsion confinement, J. Phys. Chem. B 121 (31) (2017) 7447–7454.
- [46] D. Argyris, D.R. Cole, A. Striolo, Ion-specific effects under confinement: the role of interfacial water, ACS Nano 4 (4) (2010) 2035–2042.
- [47] S. Nihonyanagi, S. Yamaguchi, T. Tahara, Direct evidence for orientational flip-flop of water molecules at charged interfaces: a heterodyne-detected vibrational sum frequency generation study, J. Chem. Phys. 130 (20) (2009) 204704
- [48] Q. Du, R. Superfine, E. Freysz, Y.R. Shen, Vibrational spectroscopy of water at the vapor/water interface, Phys. Rev. Lett. 70 (15) (1993) 2313.
- [49] C.D. Bain, Studies of adsorption at interfaces by optical techniques: ellipsometry, second harmonic generation and sum-frequency generation, Curr. Opin. Colloid Interface Sci. 3 (3) (1998) 287–292.
- [50] K.T. Nguyen, A.V. Nguyen, G.M. Evans, Interfacial water structure at surfactant concentrations below and above the critical micelle concentration as revealed by sum frequency generation vibrational spectroscopy, J. Phys. Chem. C 119 (27) (2015) 15477–15481.
- [51] R.-J. Feng, X. Li, Z. Zhang, Z. Lu, Y. Guo, Spectral assignment and orientational analysis in a vibrational sum frequency generation study of DPPC monolayers at the air/water interface, J. Chem. Phys. 145 (24) (2016) 244707.
- [52] T. Ishiyama, V.V. Sokolov, A. Morita, Molecular dynamics simulation of liquid methanol. II. Unified assignment of infrared, raman, and sum frequency generation vibrational spectra in methyl C-H stretching region, J. Chem. Phys. 134 (2) (2011).
- [53] W. Bzeih, A. Gheribi, P.M. Wood-Adams, P.L. Hayes, Dependence of the surface structure of polystyrene on chain molecular weight investigated by sum frequency generation spectroscopy, J. Phys. Chem. C (2018).
- [54] S.A. Goussous, M.T.L. Casford, S.A. Johnson, P.B. Davies, A structural and temporal study of the surfactants behenyltrimethylammonium methosulfate and behenyltrimethylammonium chloride adsorbed at air/water and air/glass interfaces using sum frequency generation spectroscopy, J. Colloid Interface Sci. 488 (2017) 365–372.
- [55] R.A. Livingstone, Y. Nagata, M. Bonn, E.H.G. Backus, Two types of water at the water-surfactant interface revealed by time-resolved vibrational spectroscopy, J. Am. Chem. Soc. 137 (47) (2015) 14912–14919.
- [56] K.T. Nguyen, T.D. Nguyen, A.V. Nguyen, Strong cooperative effect of oppositely charged surfactant mixtures on their adsorption and packing at the air–water interface and interfacial water structure, Langmuir 30 (24) (2014) 7047–7051.
- [57] M.M. Knock, C.D. Bain, Effect of counterion on monolayers of hexadecyltrimethylammonium halides at the air—water interface, Langmuir 16 (6) (2000) 2857–2865.
- [58] F. Dederichs, K.A. Friedrich, W. Daum, Sum-frequency vibrational spectroscopy of CO adsorption on Pt (111) and Pt (110) electrode surfaces in perchloric acid solution: effects of thin-layer electrolytes in spectroelectrochemistry, J. Phys. Chem. B 104 (28) (2000) 6626–6632.

- [59] B.S. Day, S.F. Shuler, A. Ducre, J.R. Morris, The dynamics of gas-surface energy exchange in collisions of Ar atoms with  $\omega$ -functionalized self-assembled monolayers, J. Chem. Phys. 119 (15) (2003) 8084–8096.
- [60] U.I. Premadasa, N.M. Adhikari, S. Baral, A.M. Aboelenen, K.L.A. Cimatu, Conformational changes of methacrylate-based monomers at the air-liquid interface due to bulky substituents, J. Phys. Chem. C 121 (31) (2017) 16888– 16902
- [61] A.A. Shahir, K.T. Nguyen, A.V. Nguyen, A sum-frequency generation spectroscopic study of the Gibbs analysis paradox: monolayer or submonolayer adsorption?, PCCP 18 (13) (2016) 8794–8805.
- [62] Y. Rao, X. Li, X. Lei, S. Jockusch, M.W. George, N.J. Turro, K.B. Eisenthal, Observations of interfacial population and organization of surfactants with sum frequency generation and surface tension, J. Phys. Chem. C 115 (24) (2011) 12064–12067.
- [63] F.M. Menger, S.A.A. Rizvi, Relationship between surface tension and surface coverage, Langmuir 27 (23) (2011) 13975–13977.
- [64] H.J. Butt, K. Graf, M. Kappl, Thermodynamics of Interfaces, Physics and Chemistry of Interfaces, 3rd ed., Wiley-VCH, Weinheim, Germany, 2004, pp. 26–41.
- [65] J.A. Mondal, V. Namboodiri, P. Mathi, A.K. Singh, Alkyl chain length dependent structural and orientational transformations of water at alcohol-water interfaces and its relevance to atmospheric aerosols, J. Phys. Chem. Lett. 8 (7) (2017) 1637–1644.
- [66] D.E. Gragson, B.M. McCarty, G.L. Richmond, Ordering of interfacial water molecules at the charged air/water interface observed by vibrational sum frequency generation, J. Am. Chem. Soc. 119 (26) (1997) 6144–6152.
- [67] M. Bielawska, A. Zdziennicka, B. Jańczuk, Comparison between surface and volumetric properties of short-chain alcohols and some classical surfactants, Annales Universitatis Mariae Curie-Sklodowska sectio AA-Chemia 71 (1) (2016).
- [68] J.A. Long, B.M. Rankin, D. Ben-Amotz, Micelle structure and hydrophobic hydration, J. Am. Chem. Soc. 137 (33) (2015) 10809–10815.
- [69] D. Yu, X. Huang, M. Deng, Y. Lin, L. Jiang, J. Huang, Y. Wang, Effects of inorganic and organic salts on aggregation behavior of cationic gemini surfactants, J. Phys. Chem. B 114 (46) (2010) 14955–14964.
- [70] J.M. Troiano, L.L. Olenick, T.R. Kuech, E.S. Melby, D. Hu, S.E. Lohse, A.C. Mensch, M. Dogangun, A.M. Vartanian, M.D. Torelli, E. Ehimiaghe, S.R. Walter, L. Fu, C.R. Anderton, Z. Zhu, H. Wang, G. Orr, C.J. Murphy, R.J. Hamers, J.A. Pedersen, F.M. Geiger, Direct probes of 4 nm diameter gold nanoparticles interacting with supported lipid bilayers, J. Phys. Chem. C 119 (1) (2015) 534–546.
- [71] A.U. Chowdhury, G.J. Taylor, V. Bocharova, R.L. Sacci, Y. Luo, W.T. McClintic, Y.-Z. Ma, S.A. Sarles, K. Hong, C.P. Collier, B. Doughty, Insight into the mechanisms driving the self-assembly of functional interfaces: moving from lipids to charged amphiphilic oligomers, J. Am. Chem. Soc. 142 (1) (2020) 290–299.
- [72] P. Bothorel, J. Belle, B. Lemaire, Theoretical study of aliphatic chain structure in mono-and bilayers, Chem. Phys. Lipids 12 (2) (1974) 96–116.
- [73] E.A. Badr, Inhibition effect of synthesized cationic surfactant on the corrosion of carbon steel in 1 M HCl, J. Ind. Eng. Chem. 20 (5) (2014) 3361–3366.
- [74] R. Fuchs-Godec, The adsorption, CMC determination and corrosion inhibition of some N-alkyl quaternary ammonium salts on carbon steel surface in 2 M H2SO4, Colloids Surf., A 280 (1–3) (2006) 130–139.